J Mater Sci (2022) 57:6212–6222

Composites & nanocomposites

Mechanism of femtosecond laser induced ultrafast demagnetization in ultrathin film magnetic multilayers

Santanu Pan[1], Fabian Ganss[2], Suryanarayan Panda[1], Gabriel Sellge[2,3], Chandrima Banerjee[4], Jaivardhan Sinha[1], Olav Hellwig[2,3], and Anjan Barman[1,*]

[1] Department of Condensed Matter Physics and Material Sciences, S N Bose National Centre for Basic Sciences, Block JD, Sector III, Salt Lake, Kolkata 700106, India
[2] Institute of Physics, Chemnitz University of Technology, Reichenhainer Straße 70, 09107 Chemnitz, Germany
[3] Institute of Ion Beam Physics and Materials Research, Helmholtz-Zentrum Dresden-Rossendorf, 01328 Dresden, Germany
[4] School of Physics, Trinity College, Dublin Dublin 2, Ireland

Received: 24 October 2021
Accepted: 12 February 2022
Published online: 14 March 2022

ABSTRACT

Ever since its discovery ultrafast demagnetization has remained one of the most intriguing research areas in magnetism. Here, we demonstrate that in [Co (t_{Co})/Pd (0.9 nm)]$_8$ multilayers, the characteristic decay time in femtosecond time-scale varies non-monotonically with t_{Co} in the range 0.07 nm $\leq t_{Co} \leq$ 0.75 nm. Further investigation reveals higher spin fluctuation at higher ratio of electron to Curie temperature to be responsible for this. Microscopic three-temperature modelling unravels a similar trend in the spin–lattice interaction strength, which strongly supports our experimental observation. The knowledge of the femtosecond magnetization decay mechanism in ultrathin ferromagnetic films is unique and important for the advancement of fundamental magnetism besides their potential applications in ultrahigh speed spintronic devices.

Introduction

Magnetic systems with large perpendicular magnetic anisotropy (PMA) have drawn tremendous attention in recent times due to their existing applications in magnetic data storage devices, e.g. hard disk drives (HDD) and spin-transfer torque magnetoresistive random access memory (STT-MRAM), as well as their potential use in magnetic race track memory, which may provide superior data storage density with nanometre sized bits, high thermal stability and ultralow bit error rate [1–5]. The ultimate efficiency of any non-volatile magnetic storage media depends on both storage density as well as the read and write time. Thin film magnetic multilayers (MMLs) having large interface induced PMA are a convenient and easy to handle model system for PMA magnetic storage media [6, 7]. However, the switching speed has still been in the nanosecond regime, which warrants the understanding and application of faster

Handling Editor: Dale Huber.

Address correspondence to E-mail: abarman@bose.res.in

https://doi.org/10.1007/s10853-022-07016-y

reversal processes [8, 9]. In the quest for an efficient and alternative method to drive the magnetization reversal in a very short time scale, a new concept of ultrafast all-optical magnetic switching has been pursued by various groups [10–13], involving both ferromagnetic and antiferromagnetic materials. However, all-optical magnetic switching is determined either by generation of an internal field due to the inverse Faraday Effect or heating near the Curie temperature (T_C) as the threshold intensities generally track with the T_C and not the other magnetic parameters. Although no direct correlation between all-optical magnetic switching and ultrafast demagnetization has been made in these materials, it will surely have a crucial role to play in the above processes. Therefore, a more controlled all-optical magnetic switching process in ferromagnetic materials demands a deeper insight into the underlying mechanism of ultrafast demagnetization.

Since its discovery in 1996 by Beaurepaire et al. [14], the mechanism of ultrafast demagnetization remains strongly debatable. Till now, many theoretical proposals as well as experimental investigations have been presented to explain its underlying physics [15–24], latest one being the development of optically induced spin transfer (OISTR) mechanism [25, 26]. In the last two decades most of the ultrafast demagnetization experiments were performed in magnetic thin films with in-plane anisotropy. Therefore, less knowledge is available for thin films with PMA, especially MMLs [27–30]. Such knowledge would be essential to the development of high-density ultrafast storage and memory devices, and thus, lead to a thriving research interest to investigate ultrafast demagnetization in PMA systems. Most of the MMLs constitute of alternating ultrathin ferromagnetic (FM) layers and heavy metal (HM) layers and the strength of PMA scales inversely with the individual FM layer thickness [31, 32]. The characteristic magnetic properties of each of these ultrathin FM layers strongly depend on its thickness [33–35]. Therefore, understanding the underlying mechanism of ultrafast spin dynamics of such PMA systems warrants a thorough investigation as a function of FM layer thickness down to the ultrathin regime, which is nontrivial.

Motivated by the above facts, we have investigated the ultrafast demagnetization in $[Co/Pd]_8$ thin film multilayers with the Co thickness (t_{Co}) being varied from a few monolayers (0.75 nm) down to the submonolayer (0.07 nm) regime. The experimentally measured demagnetization curves are analysed by using a three-temperature model-based expression [36], to extract the demagnetization time (τ_M). Further, to explain the behaviour of τ_M as a function of t_{Co}, we investigated the variation of Curie temperature (T_C) in this ultrathin regime and estimated the ratio of electron to Curie temperature in the thickness range 0.22 nm $\leq t_{Co} \leq$ 0.75 nm, which here strongly correlates with the trend of τ_M with t_{Co}.

Materials and methods

A series of [Co (t_{Co})/Pd (0.9 nm)]$_8$ MMLs with various t_{Co} values ranging from 0.07 nm to 0.75 nm have been deposited using high vacuum DC magnetron sputtering for our investigation [37]. We have used Ta (1.5 nm)/Pd (3 nm) as a seed layer system, which ensures a [111] textured growth on top of the Si substrate. An additional protective layer of Pd of thickness 1.1 nm is deposited on top of the MML stack. The values of t_{Co} are chosen to be 0.07, 0.13, 0.22, 0.36, 0.50 and 0.75 nm. The magnetic hysteresis loops are measured by polar magneto-optical Kerr effect (P-MOKE) at room temperature. The variation of the remanent magnetization of the MMLs as a function of temperature is measured using a superconducting quantum interference device (SQUID)-based vibrating sample magnetometer (SQUID-VSM). The temperature is continuously swept (10 K/min), starting at room temperature up to 625 K for t_{Co} = 0.22 nm, 0.36 nm, 0.50 nm and up to 700 K for t_{Co} = 0.75 nm. For t_{Co} = 0.75 nm the measurement is performed in a weak perpendicular external magnetic field of H = 0.5 kOe to impede domain wall motion through the MMLs before the Curie temperature is reached. The ultrafast demagnetization dynamics are probed by time-resolved magneto-optical Kerr effect (TR-MOKE) measurements in a two-colour optical pump probe setup in non-collinear geometry [38]. The second harmonic pulse (wavelength, λ = 400 nm, pulse width $\approx$ 50 fs) of a femtosecond amplified laser system (LIBRA, Coherent) is used as pump, while the time-delayed fundamental output laser (λ = 800 nm, pulse width $\approx$ 40 fs) is used as probe. The fundamental output laser beam

from LIBRA has horizontal or p-polarization. The pump and probe beams are focused on the sample surface in a non-collinear geometry by using suitable lenses with spot diameters of ~ 200 μm and ~ 100 μm, respectively. The probe beam is incident normal on the sample surface using a plano-convex lens of focal length of 25 mm and the back-reflected probe beam is collected by using the same lens and analysed using a polarized beam splitter and dual photo-detector assembly. This system has the capability to isolate the reflectivity and Kerr rotation signals and measure them simultaneously, which are subsequently plotted as a function of the delay time between pump and probe. A large external magnetic field of H = 4 kOe is applied along the surface normal to saturate the magnetization during TR-MOKE measurements. Both Kerr rotation and reflectivity signals are measured for various incident pump fluences (F = 9.5, 12.6, 15.7, 18.8 mJ/cm^2) and a fixed probe fluence (1 mJ/cm^2). The experimental data points are measured at a time interval of 40 fs ensuring high resolution and precise determination of τ_M.

Results

We have chosen all the [Co(t_{Co})/Pd (0.9 nm)]$_8$ multilayer samples with t_{Co} ranging between 0.07 nm ≤ t_{Co} ≤ 0.75 nm for our investigation. The static magnetic hysteresis loops measured by P-MOKE are presented in Fig. 1 which exhibits square hysteresis loops. On the other hand, the hysteresis loop for t_{Co} = 0.07 nm does not exhibit a square shape. To explore the ultrafast demagnetization mechanism in ultrathin film MMLs, we experimentally measured the transient change in Kerr rotation corresponding to the ultrafast drop in magnetization using a TR-MOKE setup.

The demagnetization traces for all samples at pump fluence, F = 15.7 mJ/cm^2 are plotted as a function of delay time in Fig. 2a. The raw experimental data are then fitted with a phenomenological expression, obtained by solving the coupled differential rate equations for three different temperature baths, namely electron, spin and lattice to extract the values of τ_M and fast relaxation times for the electronic system (τ_E) [36]. The analytical expression is given below:

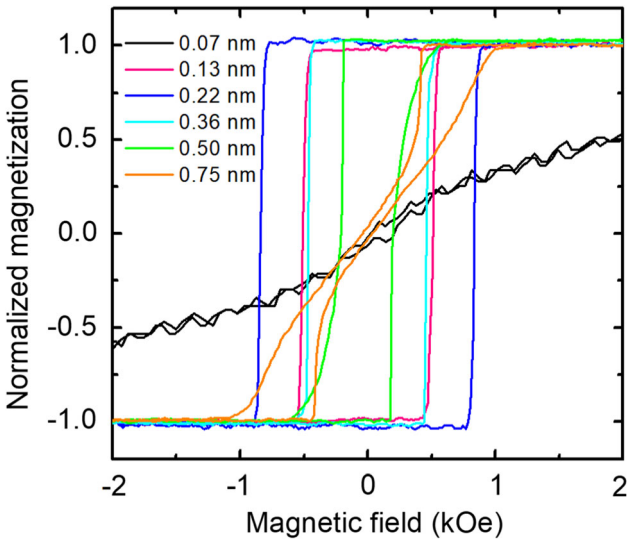

Figure 1 Magnetization versus magnetic field for all six samples. While the thickest sample (t_{Co} = 0.75 nm) starts exhibiting a labyrinth or stripe domain structure, the thinnest sample (t_{Co} = 0.07 nm) loses the perpendicular magnetic anisotropy possibly due to a discontinuous film growth.

$$\frac{-\Delta M_Z}{M_z} = \left\{ \left[\frac{A_1}{\left(\frac{t}{t_0}+1\right)^{0.5}} - \frac{(A_2\tau_E - A_1\tau_M)}{\tau_E - \tau_M} e^{-\frac{t}{\tau_M}} - \frac{\tau_E(A_1 - A_2)}{\tau_E - \tau_M} e^{-\frac{t}{\tau_E}} \right] H(t) + A_3\delta(t) \right\} \otimes G(t) \quad (1)$$

where A_1, A_2, and A_3 are constants related to the different magnetization amplitudes. $H(t)$, $G(t)$, and $\delta(t)$ denote the Heaviside step function, Gaussian function representing the laser pulse and Dirac delta function, respectively. While the ultrafast demagnetization process is primarily related to the rise in electron and spin temperature, the fast relaxation time relies on the energy transfer rate from electrons to the lattice. The values of τ_M and τ_E, as extracted from the fitting, are given in Table 1 (error bars correspond to the standard deviation of the fits to the measured data using Eq. 1).

We observe a non-monotonic variation in τ_M with t_{Co}, as shown in Fig. 2b, while overall less variation is observed in τ_E. As t_{Co} increases, τ_M increases sharply from 236 fs and exhibits a maximum value of 310 fs for t_{Co} = 0.22 nm, beyond which it systematically decreases again and drops back to 265 fs for t_{Co} = 0.75 nm. To explore the effect of pump fluence on τ_M, we have measured the ultrafast demagnetization

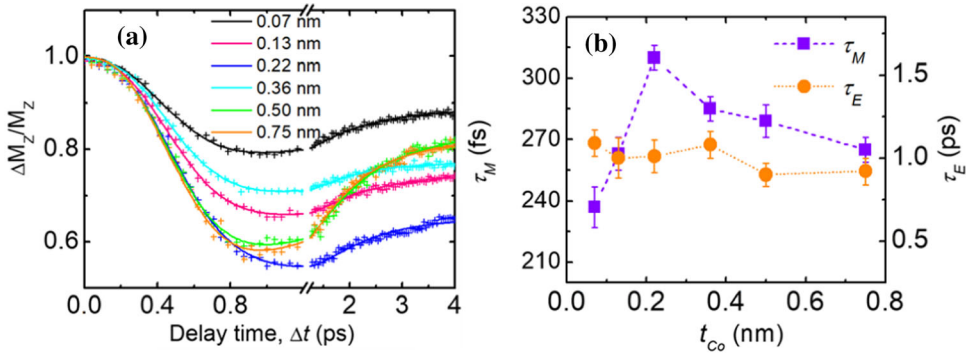

Figure 2 **a** Time-resolved magnetization dynamics for samples with different t_{Co} values for a fixed pump fluence = 15.7 mJ/cm^2 and probe fluence = 1 mJ/cm^2. The external perpendicular magnetic field was fixed at 4 kOe. Scattered symbols are experimental data and solid lines are fits to them using Eq. (1). **b** Variation of ultrafast demagnetization time (τ_M) and fast relaxation time (τ_E) with t_{Co}. Filled square and circular symbols represent the experimentally obtained values of τ_M and τ_E, respectively, while the dashed and dotted lines are guides to the eye.

Table 1 Experimentally obtained values of τ_M and τ_E for F = 15.7 mJ/cm^2 for all six samples (error bars correspond to the standard deviation of the fits to the measured data using Eq. 1)

t_{Co} (nm)	τ_M (fs)	τ_E (ps)
0.07	236 ± 9	1.09 ± 0.08
0.13	260 ± 7	1.00 ± 0.12
0.22	310 ± 5	1.01 ± 0.10
0.36	285 ± 6	1.12 ± 0.07
0.50	280 ± 7	0.90 ± 0.08
0.75	265 ± 8	0.93 ± 0.06

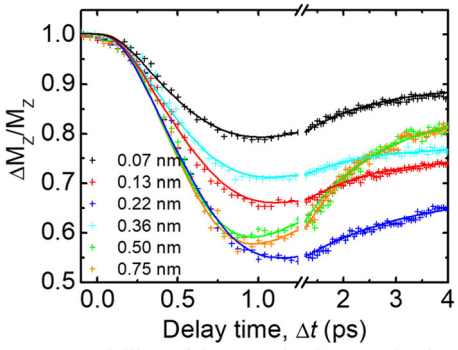

Figure 3 Modelling of time-resolved magnetization dynamics for all six samples with different t_{Co} values using coupled differential rate equations based on the three-temperature model (Eqs. 2–4). Scattered symbols represent the experimental data, whereas the solid lines represent the calculated data.

subject to various applied pump fluences. All the fluence dependent demagnetization curves are fitted with Eq. 1 and the values of the corresponding τ_M are extracted. The details of τ_M as a function of fluence are provided in the supplementary material (Fig. S1 of supplementary material). In spite of the variation of τ_M with the pump fluence, it varies in the same non-monotonic manner with the thickness of Co layer at all fluence values (Fig. S2 of supplementary material). Figure 2b also presents the variation of τ_E against Co thickness.

As shown in Fig. 3, the calculated ultrafast demagnetizations are in good agreement with the experimentally measured data. In our calculation, we have considered a linear contribution of the electronic specific heat, i.e. $C_e = \gamma T_e$. The value of γ is taken to be 0.7×10^3 Jm^{-3} K^{-2} [39]. The values of the other free parameters are listed in Table 2. Although there are three different coupling parameters, our primary concern is G_{sl}, which determines the ultrafast demagnetization time. G_{el} signifies the decay of the electronic temperature until the equilibrium is reached, and G_{es} is proportional to the maximum value of T_s. From Table 2, we can readily find that there is no significant change in the G_{el} and G_{es}, but the value of G_{sl} exhibits a monotonically decreasing trend from t_{Co} = 0.22 nm to t_{Co} = 0.75 nm. This variation strongly supports our experimental observation.

To understand the role of Curie temperature on ultrafast demagnetization, it is imperative to understand the behaviour of T_C in the ultrathin regime but it has rarely been systematically explored due to the level of measurement difficulty [40, 41]. However, to accomplish this challenging task we measured the change in remanent magnetic moment as a function of temperature (T) to estimate the value of T_C for each

Table 2 Extracted values of free parameters obtained from modelling the ultrafast demagnetization results using Eqs. (2, 3, 4)

t_{Co} (nm)	C_s (Jm^{-3} K^{-1})	C_l (Jm^{-3} K^{-1})	G_{el} (Wm^{-3} K^{-1})	G_{es} (Wm^{-3} K^{-1})	G_{sl} (Wm^{-3} K^{-1})
0.07	235×10^5	45×10^6	10×10^{17}	25×10^{17}	95×10^{17}
0.13	170×10^5	18×10^6	10×10^{17}	22×10^{17}	39×10^{17}
0.22	122×10^5	13×10^6	10×10^{17}	19×10^{17}	50×10^{17}
0.36	130×10^5	15×10^6	13×10^{17}	20×10^{17}	39×10^{17}
0.50	98×10^5	24×10^6	10×10^{17}	22×10^{17}	30×10^{17}
0.75	80×10^5	21×10^6	11×10^{17}	26×10^{17}	22×10^{17}

sample. The measured data are plotted against T as shown in Fig. 4a. The intersection of the curves with the zero magnetic moment line are pointed out by arrows and the values of T_C obtained therefrom are 510 K, 595 K, 625 K, 640 K corresponding to t_{Co} = 0.22, 0.36, 0.50, 0.75 nm, respectively. The variation of T_C as a function of t_{Co} is presented in Fig. 4b, which shows a gradually increasing exponential nature of T_C, thus agreeing quite well with earlier reports for coupled multilayer systems [41]. Here, one may note that we have presented the data corresponding to t_{Co} = 0.22, 0.36, 0.50, 0.75 nm only. This is because the Co layers become discontinuous as t_{Co} goes below the critical thickness (τ_{Co}^{Crit} ~ 0.16 nm) forming ferromagnetic Co-islands in between the Pd layers [35]. This reduces the long-range interactions as well as the coordination number of each ferromagnetic atom leading towards an ill-defined T_C. This is also reflected in the PMA values, which drop drastically below t_{Co} = 0.22 nm.

Discussion

The square shape of the P-MOKE hysteresis loops indicates the presence of strong PMA. However, towards the higher thickness regime, the shape of the loops changes, which indicates the formation of a stripe or labyrinth domain structure as usual for thicker PMA systems in order to reduce their large demagnetization energy, which indicates the loss of PMA due to a discontinuous growth of the Co layer at such a small nominal thickness. Earlier reports showed that the saturation magnetization (M_S) increases monotonically with t_{Co}, while the strength of PMA varies non-monotonically with a maximum at t = 0.22 nm [31–35, 37]. The increase in τ_M with fluence can be well explained via the enhanced spin fluctuations at more elevated temperature of the spin system [39–42]. On the other hand, though there is no drastic change in the τ_E value, a slight reduction has been observed towards the higher thickness. The thicker Co layers being more uniform than the

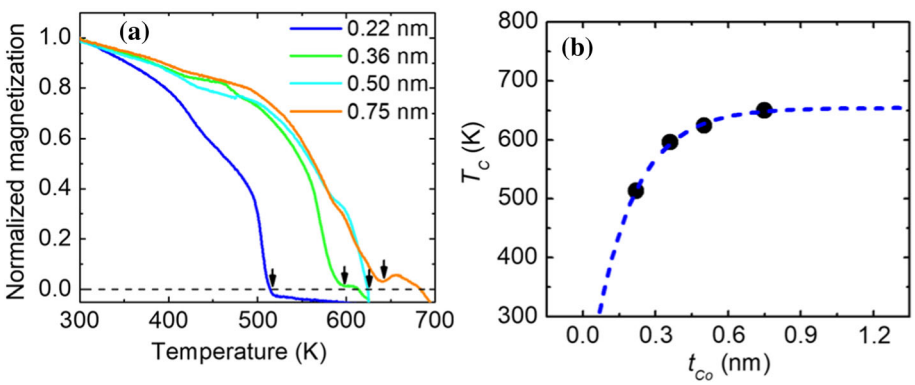

Figure 4 **a** Plots of normalized magnetization as a function of temperature (T) for t_{Co} = 0.22 nm, 0.36 nm, 0.50 nm, 0.75 nm. The Curie temperature (T_C) values are marked by arrows on the x-axis. **b** Variation of T_C with t_{Co}. Filled symbols are extracted values of T_C, while the dashed line is a guide to the eye. The dashed line is extrapolated beyond the experimental thickness range to indicate the trend of variation at lower and higher thickness regime.

thinner ones, support better energy transfer from electron and spin to lattice. This enhances the fast relaxation rate and thereby reducing the relaxation time slightly. To fully explore the microscopic details of the ultrafast demagnetization process and extract the coupling parameters among three different energy baths, i.e. electron, spin and lattice, we have modelled the experimental data by numerically solving the coupled equations [14], which are given below:

$$C_e(T_e)\frac{dT_e}{dt} = -G_{el}(T_e - T_l) - G_{es}(T_e - T_s) + P(t) \quad (2)$$

$$C_s(T_s)\frac{dT_s}{dt} = -G_{es}(T_s - T_e) - G_{sl}(T_s - T_l) \quad (3)$$

$$C_l(T_l)\frac{dT_l}{dt} = -G_{el}(T_l - T_e) - G_{sl}(T_l - T_s) \quad (4)$$

where T_e, T_s and T_l are electron, spin and lattice temperature. C_e, C_s and C_l are the electron, spin and lattice contribution to the specific heat. G_{el}, G_{es} and G_{sl} are the electron-lattice, electron-spin and spin–lattice coupling constant. $P(t)$ represents the laser power term. In the initial process, the temperature evolution of all the energy baths is calculated. Subsequently, the evolution of spin temperature is fed into the mean field theory [43], to extract the magnetization of the system at any particular temperature. The calculated transient change in magnetization is then fitted with the experimental data while keeping the different coupling constants as free parameters. In this study, we have considered uniform spatial distribution of temperature, which eliminates any heat propagation. This assumption is strongly valid in this present study. The lateral heat propagation will be negligible at the picosecond timescale as the spot diameter is quite large ($\sim$ 100 μm). Besides, there will be no longitudinal, i.e. vertically downwards to the bottom of the sample, heat transport, as the optical penetration depth (17 nm) is much larger than the total film thickness, thus causing predominantly direct interaction between the laser pulse and different magnetic and non-magnetic layers.

We now attempt to underpin the reason behind this characteristic non-monotonic behaviour of τ_M in the ultrathin film regime. To accomplish this challenge, one needs to pursue a thorough investigation of the characteristic changes of the static magnetic properties of the MML system when its thickness changes from the thin to the ultrathin range. There are different possibilities, which may lead to this kind of variation of τ_M with t_{Co}. First, as t_{Co} decreases, more discontinuities and defects are introduced at the Co/Pd interfaces, which may enhance the phonon-mediated spin-flip scattering time [44], and the ensuing τ_M. However, the declining nature of the curve below t_{Co} = 0.22 nm contradicts this possibility, and thus, rules it out. Second, a similar variation of PMA and τ_M indicates towards a possible role of the PMA in controlling τ_M. But the energy related to the PMA is $K_u \leq 1$ meV, which is too small to control the dynamics at the femtosecond timescale, which is dominated by the exchange interaction of the order of a few eV [45]. Third, Kuiper et al. have shown that the spin–orbit coupling strength of heavy metal layers plays an important role on ultrafast demagnetization in MMLs and reduces the demagnetization time [39]. They obtained a demagnetization time of 200–250 fs for Co which reduces dramatically to 60–100 fs for Co/Pt structures. We have used a Pd layer of constant thickness (0.9 nm) in the Co/Pd multilayer series which will have significantly smaller spin–orbit coupling than Co/Pt multilayers due to much smaller atomic number of Pd (46) as opposed to Pt (78). Fourth, the latest development of optically induced spin transfer mechanism (OISTR) opened up a new avenue, which can well explain the ultrafast demagnetization at early time scale (< 50 fs) [25, 26, 46]. This phenomenon is observable in multisublattice structures, such as alloys and multilayers. Moreover, the OISTR effect lasts for a few monolayers and gradually diminishes [46, 47], which may explain the non-monotonic variation of ultrafast demagnetization in our samples. However, we do not observe any initial increase in the magnetization at zero-time delay [48], the demagnetization curves do not saturate at a very early time delay ($\sim$ 50 fs) [26] either, and the constant Pd layer thickness for all samples indicates an invariance in the spin–orbit coupling [49]. Although these features are necessary, they are not sufficient to rule out the presence of OISTR effect and hence, a combination of OISTR and Curie temperature controlled ultrafast demagnetization may be present in these samples. Therefore, OISTR will control the ultrafast demagnetization in very early timescale ($\sim$ 50 fs) and the Curie temperature beyond that. However, one needs an experimental arrangement with much higher time resolution (by using an attosecond pulsed laser) to identify a very small contribution of OISTR [26],

which is beyond the scope of this study. Instead, the demagnetization at a longer time scale strongly suggests a dominant role of spin–orbit mediated spin-flip scattering in our samples [26]. Fifth, the role of t_{Co}-dependent T_C in the ultrathin regime [40, 50, 51], which has a significant influence on the ultrafast demagnetization process [31].

Now we focus to understand the behaviour of τ_M for t_{Co} = 0.07 and 0.13 nm. Although the investigation and understanding of magnetic properties of discontinuous FM thin films are rare in the literature, we propose the reduction of long-range exchange interaction to be responsible for the reduced τ_M value. In other words, as t_{Co} goes below τ_{Co}^{Crit}, only weak short-range interactions prevail inside the individual ferromagnetic clusters, and as a result, any interaction with the femtosecond laser pulse can more easily and quickly drive the ordered spin state into a non-equilibrium disordered spin state.

We now explore the variation of τ_M for 0.22 nm $\leq t_{Co} \leq$ 0.75 nm, where it declines gradually. The influence of the variation of T_e with respect to T_C on the ultrafast demagnetization process has been already reported by Münzenberg et al. [45] Here, we will substantiate our result by estimating the T_e values for the samples with t_{Co} = 0.22 nm, 0.36 nm, 0.50 nm, 0.75 nm. The temperature evolution, as obtained from Eqs. 2–4, for the sample with t_{Co} = 0.22 nm is plotted in Fig. 5a. The calculated data shows that T_e rises very fast, followed by both T_s and T_l. The coupling between the temperature baths causes rapid decay of T_e before reaching an equilibrium with spin and lattice after a few picoseconds. Figure 5b shows the evolution of T_e for the samples having t_{Co} between 0.22 and 0.75 nm. The peak values of T_e are 3300 K, 3070 K, 2875 K, 2570 K for the samples with t_{Co} = 0.22 nm, 0.36 nm, 0.50 nm and 0.75 nm, respectively. It is clear that T_e declines gradually with increasing t_{Co}, while T_C increases. Furthermore, the time-resolved reflectivity curves reveal that the change in T_e is proportional to the change in the transient reflectivity, which is consistent with earlier reports [20, 41]. More details of reflectivity curves are provided in the supplementary material (Fig. S3 of supplementary material).

Finally, to explain the underlying reason of the enhancement in τ_M with decreasing t_{Co}, we refer to the Landau-Lifshitz-Bloch equation [52]:

$$\dot{\boldsymbol{n}} = \gamma\left[\boldsymbol{n} \times \boldsymbol{H}_{eff}\right] + \frac{\gamma\alpha_{\parallel}}{n^2}\left[\boldsymbol{n} \cdot \boldsymbol{H}_{eff}\right]\boldsymbol{n} - \frac{\gamma\alpha_{\perp}}{n^2}\left[\boldsymbol{n} \times \left(\boldsymbol{n} \times \boldsymbol{H}_{eff}\right)\right] \quad (5)$$

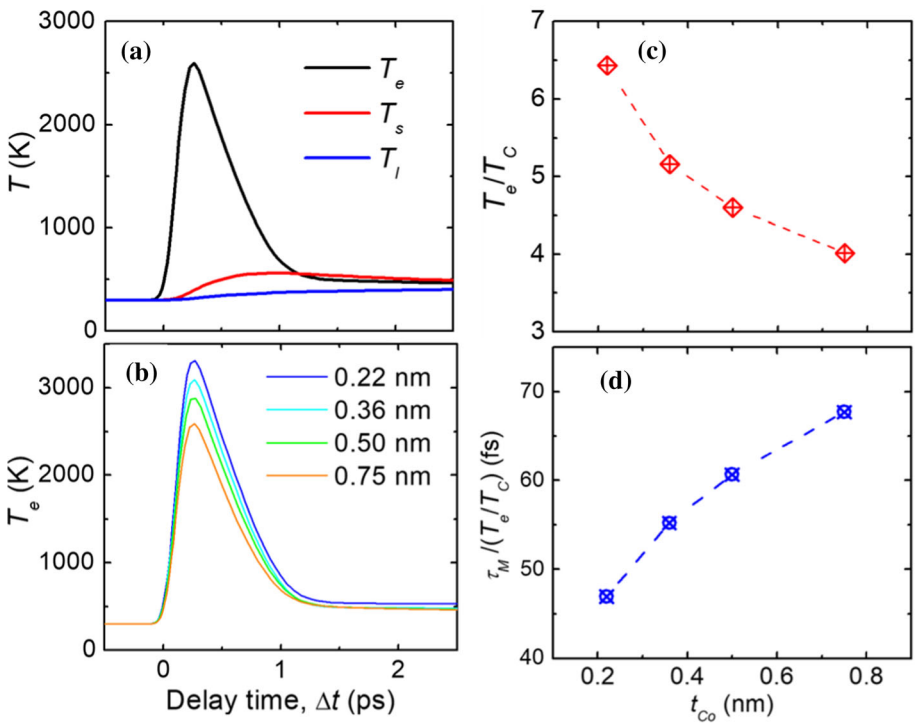

Figure 5 **a** Calculated data of evolution of electron temperature (T_e), spin temperature (T_s) and lattice temperature (T_l) as a function of time delay for the sample with t_{Co} = 0.75 nm. **b** Variation of T_e as a function of time delay for a subset of all the samples. **c** Monotonically decreasing variation of the ratio of electron to Curie temperature (T_e/T_C) with t_{Co} in the range 0.22 nm $\leq t_{Co} \leq$ 0.75 nm. **d** Variation in $\frac{\tau_M}{(T_e - T_C)}$ with t_{Co}. The symbols in both plots represent the experimentally obtained values and the dashed lines are a guide to the eye.

where $n = m/m_e$, m_e being the equilibrium magnetization, while $\alpha_{\parallel}$ and $\alpha_{\perp}$ represent longitudinal and transverse relaxation parameters. The second term on the right-hand side of Eq. 5 represents the rate of spin disorder at a given temperature. All the microscopic spin fluctuations for various length scales appear at higher temperatures resulting in a large dynamic longitudinal susceptibility ($\chi_{\parallel}$), which is inversely proportional to the strength of the exchange interaction $\left(\chi_{\parallel} \propto J^{-1}\right)$ [53]. $\chi_{\parallel}$ also holds an inversely proportional relation with the longitudinal relaxation rate $\left(\Gamma_{\parallel}\right)$ [54]. Hence, at higher temperatures it exhibits a smaller value of $\Gamma_{\parallel}$, i.e. a critical slowdown behaviour. Therefore, one may conclude that T_e rises at a faster time scale than the longitudinal relaxation time, which becomes more prominent as the temperature rises [20, 45, 54]. Hence, the response in the spin system lags the electronic system. This delayed response leads to a slowing down of the demagnetization process and enhances the value of τ_M. Now, being proportionate to the rise in T_e, both spin fluctuations and the resulting dynamic longitudinal susceptibility increase as t_{Co} decreases. This trend of variation with t_{Co} is further imprinted on the change of τ_M. Figure 5c represents the variation of T_e/T_C as a function of t_{Co}. The declining nature of this curve with the increasing t_{Co} resembles the variation of τ_M versus t_{Co} for $0.22\ \text{nm} \leq t_{Co} \leq 0.75\ \text{nm}$. In other words, as t_{Co} decreases the difference between T_e and T_C continues to increase and enhances τ_M continuously. This clearly indicates that the electron temperature is not the only factor to determine ultrafast demagnetization time in ultrathin films, but the ratio of electron to Curie temperature is also imperative. Furthermore, the monotonically increasing nature of $\frac{\tau_M}{\left(\frac{T_e}{T_C}\right)}$ with t_{Co}, as shown in Fig. 5d, implies that the electron temperature has a more prominent effect on ultrafast demagnetization time towards higher Co layer thickness.

Conclusions

We have experimentally investigated the laser induced ultrafast demagnetization in [Co (t_{Co})/Pd (0.9 nm)]$_8$ thin film MMLs having large PMA, with t_{Co} varying in the range $0.07\ \text{nm} \leq t_{Co} \leq 0.75\ \text{nm}$ and explored the possible mechanisms behind the ultrafast drop in magnetization within a few hundreds of femtoseconds in both sub-monolayer and few monolayer thickness regimes. The experimental data have been analysed using the three-temperature model and the values of corresponding coupling constants have been estimated. The variation in the spin–lattice coupling constant strongly supports our experimental observation. The reduction in τ_M with decreasing Co layer thickness in the sub-monolayer regime appears due to the lack of long-range interaction in the increasingly discontinuous Co layers. On the other hand, as t_{Co} increases beyond one continuous monolayer (which we think is occurring at a nominal Co thickness of about 0.22 nm), we also observe a gradual decline in τ_M with increasing t_{Co}. Subsequently, we have found that as t_{Co} increases the corresponding T_C increases and T_e decreases. Thus, we understand that the higher the T_e and its ratio with T_C, the more is the strength of spin fluctuation leading to a reduced value of τ_M, as we decrease the Co layer thickness within the continuous film regime. We have identified the crucial role of FM layer thickness dependent T_C on ultrafast demagnetization in the ultrathin regime. Our results open new possibilities to control the ultrafast demagnetization in thin film magnetic multilayers down to sub-monolayer FM thickness in one of the most convenient and easy to handle model systems for future magnetic recording devices. Importantly, we have been able to tune the demagnetization time, an essential parameter for future ultrafast magnetic storage and memory devices.

Acknowledgements

We acknowledge S. N. Bose National Centre for Basic Sciences (SNBNCBS) for funding under Projects Nos. SNB/AB/12-13/96 and SNB/AB/18-19/211 and Nano Mission, Department of Science and Technology, Govt. of India for funding under Grant No. DST/NM/TUE/QM-3/2019-1C-SNB. SNP acknowledges SNBNCBS for a senior research fellowship.

Declarations

Conflict of interest The authors declare no potential conflict of interest or competing interest.

Supplementary Information: The online version contains supplementary material available at https://doi.org/10.1007/s10853-022-07016-y.

References

[1] Plumer ML, Van Ek J, Weller D (2012) The physics of ultra-high-density magnetic recording. Springer Science & Business Media, Berlin Heidelberg 41:1–353

[2] Ouchi K (2001) Recent advancements in perpendicular magnetic recording. IEEE Trans Magn 37:1217–1222

[3] Chatterjee J, Chavent A, Fettar F, Auffret S, Ducruet C, Joumard I, Vila L, Sousa RC, Prejbeanu L, Dieny B (2019) Reduced thermal variation of perpendicular magnetic anisotropy in magnetically stiffened dual-W composite storage layer for spin-transfer-torque magnetic random-access memory. Phys Rev Appl 12:044043

[4] Kent AD (2010) Perpendicular all the way. Nat Mater 9:699–700

[5] Parkin SSP, Hayashi M, Thomas L (2008) Magnetic domain-wall racetrack memory. Science 320:190–194

[6] Ochiai Y, Hashimoto S, Aso K (1989) Co/Pt and Co/Pd ultrathin multilayered films as new magneto-optical recording materials. IEEE Trans Magn 25:3755–3756

[7] Kaneko M (1995) J Magn Magn Mater 148:351–356

[8] Tudosa I, Stamm C, Kashuba AB, King F, Siegmann HC, Stöhr J, Ju G, Lu B, Weller D (2004) The ultimate speed of magnetic switching n granular magnetic media. Nature 428:831–833

[9] Back CH, Allenspach R, Weber W, Parkin SSP, Weller D, Garwin EL, Siegmann HC (1999) Minimum field strength in precessional magnetization reversal. Science 285:864–867

[10] Kimel AV, Kirilyuk A, Usachev PA, Pisarev RV, Balbashov AM, Raising T (2005) Ultrafast non-thermal control of magnetization by instantaneous photomagnetic pulses. Nature 435:655–657

[11] Stanciu CD, Hansteen F, Kimel AV, Kirilyuk A, Tsukamoto A, Itoh A, Rasing T (2007) All-optical magnetic recording with circularly polarized light. Phys Rev Lett 99:047601

[12] Lambert CH, Mangin S, Varaprasad BSDCS, Takahashi YK, Hehn M, Cinchetti M, Malinowski G, Hono K, Fainman Y, Aeschlimann M, Fullerton EE (2014) All-optical control of ferromagnetic thin films and nanostructures. Science 345:1337–1340

[13] Stupakiewicz A, Szerenos K, Davydova MD, Zvezdin KA, Kirilyuk A, Kimel AV (2019) Selection rules for all-optical magnetic recording in iron garnet. Nat Commun 10:612

[14] Beaurepaire E, Merle JC, Daunois A, Bigot JY (1996) Ultrafast spin dynamics in ferromagnetic nickel. Phys Rev Lett 76:4250–4253

[15] Steiauf D, Fähnle M (2009) Eliott-Yafet mechanism and the discussion of femtosecond magnetization dynamics. Phys Rev B 79:140401

[16] Cinchetti M, Albaneda M, Hoffmann D, Roth T, Wustenberg JP, Krauβ M, Andreyev O, Schneider HC, Bauer M, Aeschlimann M (2006) Spin-flip processes and ultrafast magnetization dynamics in Co: unifying the microscopic and macroscopic view of femtosecond magnetism. Phys Rev Lett 97:177201

[17] Battiato M, Carva K, Oppeneer PM (2010) Superdiffusive spin transport as a mechanism of ultrafast demagnetization. Phys Rev Lett 105:027203

[18] Eschenlohr A, Battiato M, Maldonado P, Pontius N, Kachel T, Holldack K, Mitzner R, Fohlisch A, Oppeneer PM, Stamm C (2013) Ultrafast spin transport as key to femtosecond demagnetization. Nat Mater 12:332–336

[19] Rudolf D, La-O-Vorakiat C, Battiato M, Adam R, Shaw JM, Turgut E, Maldonado P, Mathias S, Grychtol P, Nembach HT, Silva TJ, Aeschlimann M, Kapteyn HC, Murnane MM, Schneider CM, Oppeneer PM (2012) Ultrafast magnetization enhancement in metallic multilayers driven by superdiffusive spin current. Nat Commun 3:1037

[20] Atxitia U, Chubykalo-Fesenko O, Walowski J, Mann A, Münzenberg M (2010) Evidence for thermal mechanisms in laser-induced femtosecond spin dynamics. Phys Rev B 81:174401

[21] Chen Z, Wang LW (2019) Role of initial magnetic disorder: a time-dependent ab-initio study of ultrafast demagnetization mechanisms. Science Adv 5:eaau8000

[22] Mathias S, La-O-Vorakiat C, Grychtol P, Granitzka P, Turgut E, Shaw JM, Adam R, Nembach HT, Siemens ME, Eich S, Schneider CM, Silva TJ, Aeschlimann M, Murnane MM, Kapteyn HC (2012) Probing the timescale of exchange interacion in a ferromagnetic alloy. Proc Natl Acad Sci USA 109:4792–4797

[23] Chen Z, Luo JW, Wang LW (2019) Revealing angular momentum transfer channels and timescales in the ultrafast demagnetization process of ferromagnetic semiconductors. Proc Natl Acad Sci USA 116:19258–19263

[24] Chen C, Tao Z, Carr A, Matyba P, Szilvasi T, Emmerich S, Piecuch M, Keller M, Zusin D, Eich S, Rollinger M, You W, Mathias S, Thumm U, Mavrikakis M, Aeschlimann M, Oppeneer PM, Kapteyn HC, Murnane MM (2017) Distinguishing attosecond electron-electron scattering and screening in transition metals. Proc Natl Acad Sci USA 114:E5300–E5307

[25] Hofherr M, Hauser S, Dewhurst JK, Tengdin P, Sakshath S, Nembach HT, Weber ST, Shaw JM, Silva TJ, Kaptyen HC, Cinchetti M, Rethfeld B, Murnane MM, Steil D, Stadmuller B, Sharma S, Aeschlimann M, Mathias S (2020) Ultrafast optically induced spin transfer in ferromagnetic alloys. Science Adv 6:eaay8717

[26] Siegrist F, Gessner JA, Ossiander M, Denker C, Chang YP, Schroder MC, Guggenmos A, Cui Y, Walowski J, Martens U, Dewhurst JK, Kleineberg U, Munzenberg M, Sharma S, Schultze M (2019) Light-wave dynamics control of magnetism. Nature 571:240–244

[27] Pan S, Hellwig O, Barman A (2018) Control coexcitation of direct and indirect ultrafast demagnetization in Co/Pd multilayers with large perpendicular magnetic anisotropy. Phys Rev B 98:214436

[28] Vodungbo B, Gautier J, Lambert G, Sardinha AB, Lozano M, Sebban S, Ducousso M, Bouto W, Li K, Tudu B, Tortarolo M, Hawaldar R, Delaunay R, Lopez-Flores V, Arabski J, Boeglin C, Merdji H, Zeitoun P, Luning J (2012) Laser-induced ultrafast demagnetization in the presence of a nanoscale magnetic domain network. Nat Commun 3:999

[29] Shim JH, Ali Syed A, Kim CH, Lee KM, Park SY, Jeong JR, Kim DH, Eon Kim D (2017) Ultrafast giant magnetic cooling effect in ferromagnetic Co/Pt multilayers. Nat Commun 8:796

[30] Bergeard N, Hehn M, Mangin S, Lengaigne G, Montaigne F, Lalieu MLM, Koopmans B, Malinowski G (2016) Hot-electron-induced ultrafast demagnetization in Co/Pt multilayers. Phys Rev Lett 117:147203

[31] Pal S, Rana B, Hellwig O, Thomson T, Barman A (2011) Tunable magnonic frequency and damping in $[Co/Pd]_8$ multilayers with variable Co layer thickness. Appl Phys Lett 98:082501

[32] Fallarino L, Oelschlägel A, Arregi JA, Bashkatov A, Samad F, Böhm B, Chesnel K, Hellwig O (2019) Control of domain structure and magnetization reversal in thick Co/Pt multilayers. Phys Rev B 99:024431

[33] Miura K, Kimura H, Imanaga S, Hayafuji Y (1992) Magnetic interaction between Co layers and Pd layers in Co/Pd multilayers. J Appl Phys 72:4826–4829

[34] Hashimoto S, Ochiai Y, Aso K (1990) Film thickness dependence of magneto-optical and magnetic properties in Co/Pt and Co/Pd multilayers. J Appl Phys 67:4429–4431

[35] Charilaou M, Bordel C, Berche PE, Maranville BB, Fischer P, Hellman F (2016) Magnetic properties of ultrathin discontinuous Co/Pt multilayers: comparison with short-range ordered and isotropic $CoPt_3$ films. Phys Rev B 93:224408

[36] Malinowski G, Dalla Longa F, Rietjens JHH, Paluskar PV, Huijink R, Swagten HJM, Koopmans B (2008) Control of speed and efficiency of ultrafast demagnetization by direct transfer of spin angular momentum. Nat Phys 4:855–858

[37] Hellwig O, Hauet T, Thomson T, Dobisz E, Risner-Jamtgaard JD, Yaney D, Terris BD, Fullerton EE (2009) Coercivity tuning in Co/Pd multilayer based bit patterned media. Appl Phys Lett 95:232505

[38] Barman A, Sinha J (2018) Spin dynamics and damping in ferromagnetic thin films and nanostructures. Springer International Publishing AG, Gewerbestrasse

[39] Kuiper KC, Roth T, Schellekens AJ, Schmitt O, Koopmans B, Cinchetti M, Aeschlimann M (2014) Spin-orbit enhanced demagnetization rate in Co/Pt-multilayers. Appl Phys Lett 105:202402

[40] Zhang R, Willis RF (2001) Thickness-dependent Curie temperatures of ultrathin magnetic films: effect of the range of spin-spin interactions. Phys Rev Lett 86:2665–2668

[41] Van Kesteren HW, Zeper WB (1993) Controlling the Curie temperature of Co/Pt multilayer magneto-optical recording media. J Magn Magn Mater 120:271–273

[42] Kuiper KC, Malinowski G, Longa FD, Koopmans B (2011) Unifying ultrafast demagnetization and intrinsic Gilbert damping in Co/Ni bilayers with elctronic relaxation near the Fermi surface. J Appl Phys 109:07D316

[43] Koopmans B (2007) Handbook of magnetism and advanced magnetic materials. Wiley, New York

[44] Bigot JY, Vomir M, Beaurepaire E (2009) Coherent ultrafast magnetism induced by femtosecond laser pulses. Nat Phys 5:515–520

[45] Mendil J, Nieves P, Chubykalo-Fesenko O, Walowski J, Santos T, Pisana S, Münzenberg M (2014) Resolving the role of femtosecond heated electrons in ultrafast spin dynamics. Sci Rep 4:3980

[46] Dewhurst JK, Elliott P, Shallcross S, Gross EKU, Sharma S (2018) Laser-induced intersite spin transfer. Nano Lett 18:1842–1848

[47] Golias E, Kumberg I, Gelen I, Thakur S, Gordes J, Hosseinifar R, Guillet Q, Dewhurst JK (2021) Ultrafast optically induced ferromagnetic state in an elemental ferromagnet. Phys Rev Lett 126:107202

[48] Steil D, Walowski J, Gerhard F, Kiessling T, Ebke D, Thomas A, Kubota T, Oogane M, Ando Y, Otto J, Mann A, Hofherr M, Elliott P, Dewhurst JK, Reiss G, Molenkamp L, Aeschlimann M, Cinchetti M, Munzenberg M, Sharma S, Mathias S (2020) Efficiency of ultrafast optically induced spin transfer in Heusler compounds. Phys Rev Res 2:023199

[49] Willems F, Schmising CVK, Struber C, Schick D, Engel DW, Dewhurst JK, Elliott P, Sharma S, Eisebitt S (2020) Optical inter-site spin transfer probed by energy and spin-resolved transient absorption spectroscopy. Nat Commun 11:871

[50] Bruno P (1991) Theory of the Curie temperature of Co-based ferromagnetic ultrathin films and multilayers. J Magn Soc Jpn 15:15–20

[51] Schneider CM, Bressler P, Schuster P, Kirschner J, Miguel JJ, Miranda R (1990) Curie temperature of ultrathin films of fcc-cobalt epitaxially grown on atomically flat Cu (100) surfaces. Phys Rev Lett 64:1059–1062

[52] Atxitia U, Chubykalo-Fesenko O (2011) Ultrafast magnetization dynamics rates within the Landau-Lifshitz-Bloch model. Phys Rev B 84:144414

[53] Chubykalo-Fesenko O, Nowak U, Chantrell RW, Garanin D (2006) Dynamic approach for micromagnetics close to the Curie temperature. Phys Rev B 74:094436

[54] Atxitia U, Chubykalo-Fesenko O, Kazantseva N, Hinzke D, Nowak U, Chantrell RW (2007) Micromagnetic modeling of laser-induced magnetization dynamics using the Landau-Lifshitz-Bloch equation. Appl Phys Lett 91:232507